Conductance quantization and dequantization in gold nanowires due to multiple reflection at the interface

Yoshihiko Kurui,[1] Yoshifumi Oshima,[2,3] Masakuni Okamoto,[4,*] and Kunio Takayanagi[1,3,†]

[1]*Department of Condensed Matter Physics, Tokyo Institute of Technology, 2-12-1 Oh-okayama, Meguro-ku, Tokyo 152-8551 Japan*

[2]*Department of Materials Science and Engineering, Tokyo Institute of Technology, 4259 Nagatsuta, Midori-ku, Yokohama 226-8502 Japan*

[3]*CREST, Japan Science and Technology Corporation, Kawaguchi, Saitama 332-0012, Japan*

[4]*Mechanical Engineering Research Laboratory, Hitachi Ltd. 832-2 Horiguchi, Hitachinaka, Ibaraki 312-0034, Japan*

(Received 28 November 2008; revised manuscript received 15 February 2009; published 9 April 2009)

The conductance of gold ⟨110⟩ nanowires was measured, along with simultaneous observation of their atomic structure in a transmission electron microscope. The conductance histogram obtained from 300 thinning processes of the nanowires showed a series of peaks whose conductance values increased nearly in steps of the conductance quantum, $G_0=2e^2/h$. However, thick nanowires above $10G_0$ showed dequantization, where the increment was only $0.9G_0$. The structure for each peak was found to be either an atomic sheet or a hexagonal prism. The number of conductance channels calculated for each determined atomic structure by first-principles theory, coincided well with the peak index in the conductance histogram. The observed decrease in the conductance from the quantized number of conductance channels was explained by partial transmission of electrons due to the multiple reflection at the interfaces between the nanowire and the electrodes. The present study shows that the ⟨110⟩ nanowires behave as ballistic conductors, and a conductance peak appears whenever the conductance channel is open one by one.

DOI: 10.1103/PhysRevB.79.165414 PACS number(s): 73.63.−b, 68.37.Lp, 73.40.Jn

Metal atomic contacts have attracted significant interest because of quantized conductance even at room temperature.[1] Conductance of metal contact changes in steps, while it is mechanically stretched at a constant bias voltage.[2–4] Such a time evolution experiment has suggested conductance quantization, since the step height, prior to breaking, follows the conductance quantum, $G_0=2e^2/h$. The steps however appear irregularly in the various experiments. Conductance histograms constructed from a large number of conductance curves give statistical reliability to time evolution experiments of conductance. Conductance histograms reported for a variety of metal contacts show a series of peaks in the vicinity of integer multiples of G_0; alkali metals of Na,[4,5] Li, and K (Ref. 5) show peaks at around 1, 3, 5, and $6G_0$, while Au,[6–11] Ag,[9,11] and Cu (Refs. 7 and 11) show peaks close to $1G_0$, $2G_0$, $3G_0$, and $4G_0$. Such preferred integer peaks suggest quantization of the conductance,[12] although noble metals and alkali metals exhibit different selection rules for the conductance quantum. Conductance experiments carried out for other metals such as Al,[13,14] Pt,[15] and Nb (Ref. 16) show more complicated results.

The evolution of gold contacts has been investigated using molecular-dynamics simulations.[17–23] Simultaneous observations of structure and conductance using high-resolution transmission electron microscope (TEM) have clarified how preferred structures evolve at a gold contact, in relation to their conductance values; a single and double chain, respectively, have values of $1G_0$ and $2G_0$.[24] The relation between structure and conductance has also been studied theoretically,[21,25,26] in conjunction with TEM observation. Together with recent TEM observation of zigzag atomic chains,[27] conductance quantization has been verified for atomic chains.

Conductance histograms of thick nanowires (NW) of apparent conductance values above $10G_0$ are chiefly studied by mechanically controllable breaking junction method, and show that a series of peaks has a regular period in the square root of the conductance value, $\sqrt{G}$.[28–30] Since the conductance changes whenever the atomic structure changes at metal contacts,[31] unstable structures cannot yield preferred peaks in conductance histograms. Then a proposition is given that the peaks reflect merely evolution of the preferred atomic geometry.[28–30] As a preferred and stable geometry, an atomic-shell structure model has been proposed.[32] The atomic-shell structure is thought to have hexagonal prism cross sections[33,34] and yields peaks each time the surface layer of the lateral face is removed in the thinning process in accordance with the regular period in $\sqrt{G}$. A recent TEM report on gold nanowires with the ⟨110⟩ orientation differs from the $\sqrt{G}$ regulation, verifying an increment of the conductance value in step of the conductance quantum.[35]

A question if the orientation of nanowire, such as the ⟨110⟩, ⟨111⟩, or ⟨100⟩ orientation, may contaminate the peaks in the conductance histogram is an important issue before analyzing the conductance histogram in detail. Orientation-dependent structures have been reported by electron microscopy studies.[34,36,37] Ugarte and co-workers[34,36] observed that thin gold contacts had different structures depending on the orientation, ⟨110⟩, ⟨111⟩ or ⟨100⟩, of the electrode. They pursued conductance calculations separately, and proposed a possible scenario where their observed atomic structures gave different conductance histograms for the three orientations. Simultaneous observation of structure and conductance for thicker gold contacts at each electrode orientation[37] showed obvious orientation dependence. The study revealed that a series of long free standing nanowires, ca., 1 nm, formed at the ⟨110⟩ orientation (hereafter called ⟨110⟩ nanowire) yielded sharp peaks at integer multiples of G_0. On the other hand, broad peaks were obtained for the short necked [111] and [100] contacts.

Lately, a new twist has evolved. Dreher *et al.*[23] showed a theoretical result wherein the sum of several conductance channels of partial transmission gave apparent integer multiples of the conductance quantum even in the case of the gold contact. In fact, partial transmission determines the conductance for *sp* metals such as Al (Refs. 13 and 14) and transition metals such as Pt (Ref. 15) and Nb.[16] Taking all the arguments into account, orientation, atomic structure, and partial transmission of conductance channels operate on the conductance histogram even for metals with *s* electrons. Discrimination of these factors is necessary to address the issue of how the preferred conductance or structure is selected at the metal contact, particularly for gold nanowire. Understanding how the conductance quantization or dequantization is caused for free-standing nanowires becomes important issue to be addressed for device application.[38]

In this study, we simultaneously observed conductance and the atomic structure of the gold ⟨110⟩ nanowires formed at gold atomic contacts using a TEM fitted with a scanning tunneling microscope (STM). The conductance histogram obtained from many thinning processes showed peaks in the vicinity of each integer multiple of the conductance quantum, G_0. We determined the atomic structures that yielded the peaks. The peak index accorded with the number of conductance channels, which was calculated for the structure.

This paper is organized as follows. Experimental details are given in Sec. II. The conductance histogram of the gold ⟨110⟩ nanowires is shown in Sec. II A, the gold atomic sheet, in Sec. II B, gold ⟨110⟩ nanowires with the (n,m,l) hexagonal cross section, in Sec. II C and ballistic transport inside the gold ⟨110⟩ nanowire, in Sec. II D. The theoretical calculations of the number of conductance channels are shown in Sec. III A and comparison with the experimental results, in Sec. III B. The number of conductance channels, partial transmission probability and stable gold ⟨110⟩ nanowire are discussed in Sec. IV. Our conclusions are presented in Sec. V. In this paper, we have described details on a new aspect of conductance quantization of gold ⟨110⟩ nanowires, which was briefly reported in our previous papers.[27,35]

I. EXPERIMENTAL METHOD

We fabricated gold ⟨110⟩ nanowires at room temperature and measured conductance values, using our homemade STM holder working in a TEM (JEM-2000VF) at 10^{-7} Pa.[37] The central position of a gold wire (0.25 mm diameter) was etched chemically to a bottle-neck shape. The gold wire was mechanically pulled apart on the STM holder to form electrodes. Subsequently the electrodes were brought to contact each other and pulled apart cyclically, until a thin gold nanowire was fabricated between the electrodes. Structural changes in a nanowire were observed *in situ* using the TEM, and the conductance change was measured simultaneously. TEM images were recorded at a rate of 30 frames/s, while the conductance was measured at 3 kHz at a bias voltage of 13 mV. The conductance was normalized by the conductance quantum G_0, that is, $g=G/G_0$. The electric current passing through the nanowire with a cross-sectional area of 1 nm^2 was about 10 μA, while the imaging electrons had an intensity of 0.2 pA/nm^2. The measured conductance values did not depend on whether the contact was illuminated by the imaging electron beam or not. Gold contacts were grown (elongated) parallel to the ⟨110⟩, ⟨111⟩, or ⟨100⟩ direction of the electrode. The orientation of each contact was determined from the lattice fringes observed in TEM images *in situ* while fabrication. Since lattice fringes can be observed at the Bragg reflection condition, only a small fraction (ca. about 10%) of contacts showed lattice fringes enabling orientation determination. The number of contacts having the ⟨110⟩ orientation was 300. The ⟨111⟩ and ⟨100⟩ contacts were about 800 and 150, respectively. The ⟨110⟩ nanowires of 1–3 nm in length had the face-centered-cubic structure at the beginning of thinning, and showed plateaus in their conductance traces. Long ⟨110⟩ nanowires (≥5 nm) of multishell structures[39–41] were fabricated a few times. The contacts were almost broken before they reached to 5 nm because of insufficient diffusion toward the constriction from the electrodes. The ⟨111⟩ and ⟨100⟩ contacts had bottlenecked configuration, showing no apparent plateaus. Here we report the conductance and structures of the ⟨110⟩ nanowires shorter than 5 nm.

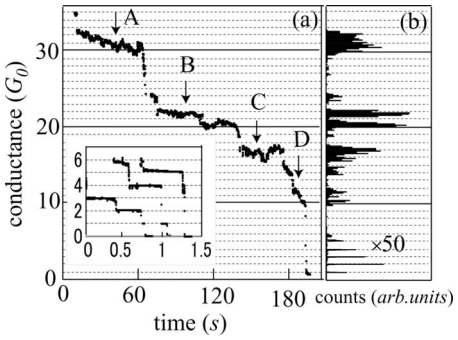

FIG. 1. (a) Time evolution of conductance for a gold ⟨110⟩ nanowire during the thinning process, and (b) conductance histogram obtained for (a). Inset in (a) shows three examples of time evolution for very thin gold ⟨110⟩ nanowires, whose conductance histogram is shown in (b). Note that flat plateaus in (a) give sharp peaks at $1G_0$, $2G_0$, $3G_0$, and $4G_0$ in (b).

II. EXPERIMENTAL RESULTS

A. Conductance histogram of gold ⟨110⟩ nanowire

Figure 1(a) shows a typical time evolution of a conductance curve for a ⟨110⟩ nanowire. The conductance changes in steps, consisting of plateaus and jumps. The conductance plateaus around $g=22$, 20, 17, 12, 10, and 1 yields conspicuous peaks in the histogram shown in Fig. 1(b). *In situ* TEM images corresponding to the conductance change are shown in Fig. 2. As will be explained later, the network image of $(\bar{1}11)$ lattice fringes shows that the [110] direction is parallel to the wire axis (inclined 30° from the plane of the TEM image). The width of the nanowire, which is known from the number of $(\bar{1}11)$ lattice planes, decreases one by one from (a) to (d) in Fig. 2. From time coincidence between the TEM images and conductance curve, the nanowires in Figs.

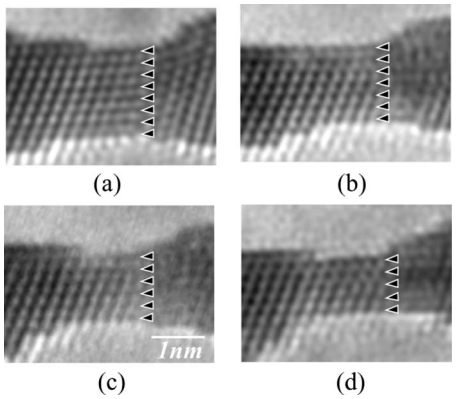

FIG. 2. A series of TEM images during the thinning process of a gold ⟨110⟩ nanowire. TEM images (a)–(d) were image frames, respectively, at A–D in Fig. 1(a). The triangular arrow heads indicate $(\bar{1}11)$ lattice planes. Note that the number of $(\bar{1}11)$ lattice planes decreases one by one from (a) to (d). See also Figs. 7(a) and 7(b).

2(a)–2(d) are known to have conductance values at A-D in Fig. 1; $g=31$, 22, 17, and 12, respectively. The inset in Fig. 1(a) shows three examples of the time-evolution curves for thin ⟨110⟩ nanowires. In each curve, a series of plateaus appears at integer multiples of the conductance quantum; $g=3,2,1$; $g=6,4,1$; $g=5$ and 4. Because of the constant plateaus, the conductance histogram in Fig. 1(b) shows sharp peaks at integer multiples of the conductance quantum.

Figure 3(a) shows a conductance histogram constructed from 300 time-evolution curves of the gold ⟨110⟩ nanowires. Conductance peaks are clearly recognizable. 30 peaks are marked by arrow heads. Some of them appear in the vicinity of integral multiples of the conductance quantum. However, some are not coincident with them. Figure 3(b) plots the conductance, g, in relation to the peak index, N_p, in the histogram of Fig. 3(a). Since a linear relation, $g=N_p$, holds for small g values, the conductance increases one-by-one as the peak index increases. The conductance values, however, start deviating above $g=10$ from the linear line. In the following sections, we present experimental and theoretical analysis to address this failure of the conductance quantization, or, dequantization.

B. Conductance of gold atomic sheets

Figure 4 shows a time evolution of conductance, wherein conductance plateaus appear in the vicinity of $g=4$, 3, 2 and 1. The series of TEM images in Figs. 5(a)–5(d) represent structures giving $g=4,3,2,1$, respectively. The electrode was not stretched. The nanowire is thinned by diffusion of atoms from the nanowire portion to the electrode one. The nanowire seen in Fig. 5(d), yielding $g=1$ just prior to breakup, is a single chain of gold atoms.[24,42] The gold atoms are seen as dots in the dark line connecting the apices of the electrodes. We find that the contrast of the dark dots become less intense from Figs. 5(b)–5(d) in order, as shown by the intensity profile in the right column in Fig. 5; the relative contrast is 2.6 ± 0.2, 1.8 ± 0.1, and 1, respectively, for the

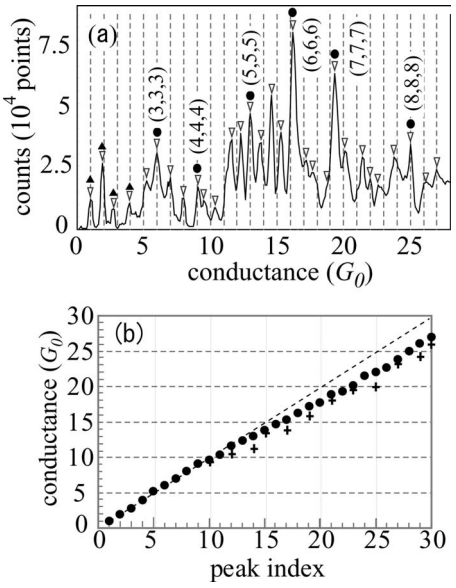

FIG. 3. (a) Conductance histogram of a gold ⟨110⟩ NW from 300 thinning processes. The peaks marked by solid triangles are for the atomic chain or sheet structure. Those marked by solid circles are for hexagonal (n,n,n) structures $(n=3-8)$. The open triangles are for the hexagonal (n,m,l) structures (see text). (b) Plots of conductance values $(g=G/G_0)$ at the peaks in (a) in relation to the peak index (N_p). The dotted line represents a linear relationship, $g=N_p$. Crosses indicate the conductance calculated for cylindrical nanowire taking partial transmission probability into account.

three cases. Since the relative contrast depends on the number of gold atoms aligned along the electron-beam direction,[43] we conclude that three atomic chains are superposed along the beam direction to give the observed image contrast in Fig. 5(b), two in Fig. 5(c), and one in Fig. 5(d). Similarly, in Fig. 5(a), two atomic chains are superposed along the electron-beam direction.

The measured distance between the dark dots, indicated by the arrows in Fig. 5, was found to be $d=0.24\pm0.02$ nm during thinning process. Since the distance is smaller than the gold dimer bond (0.248 nm), the chain must be inclined by some angle θ from the plane of the TEM image. Taking this inclination of the chain and also the number of chains aligned in the beam direction into account, structure models are constructed, as shown in Figs.

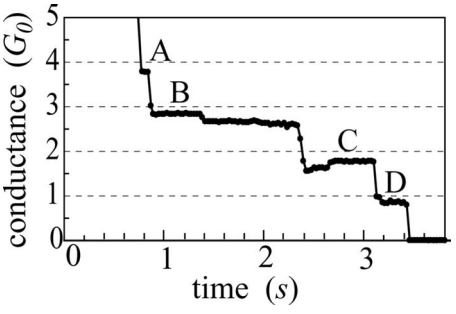

FIG. 4. Typical time evolution of conductance in gold ⟨110⟩ NW during the thinning process until breakage. Also see TEM images in Fig. 5.

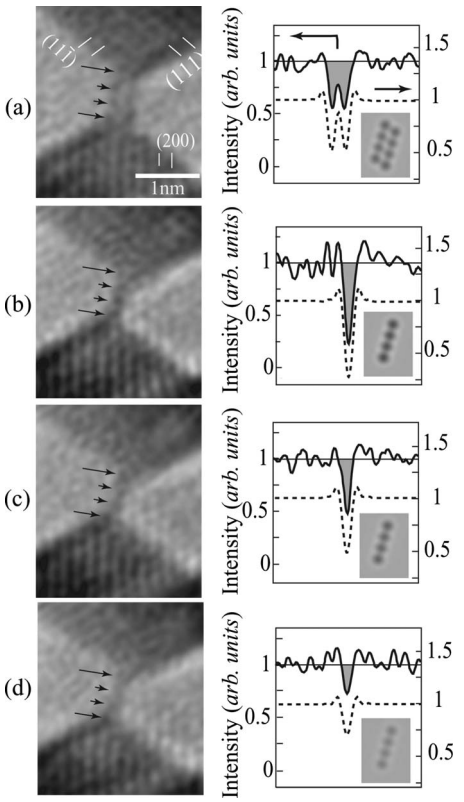

FIG. 5. A series of TEM images for the thinning process in Fig. 4. Dark dots shown by the arrows are images of gold atoms, or atomic columns. Solid curves in the right-hand-side panels display intensity profiles of the dark dots in (a). Dotted curves display profiles of the simulated images in the insets (see structure models in Fig. 6).

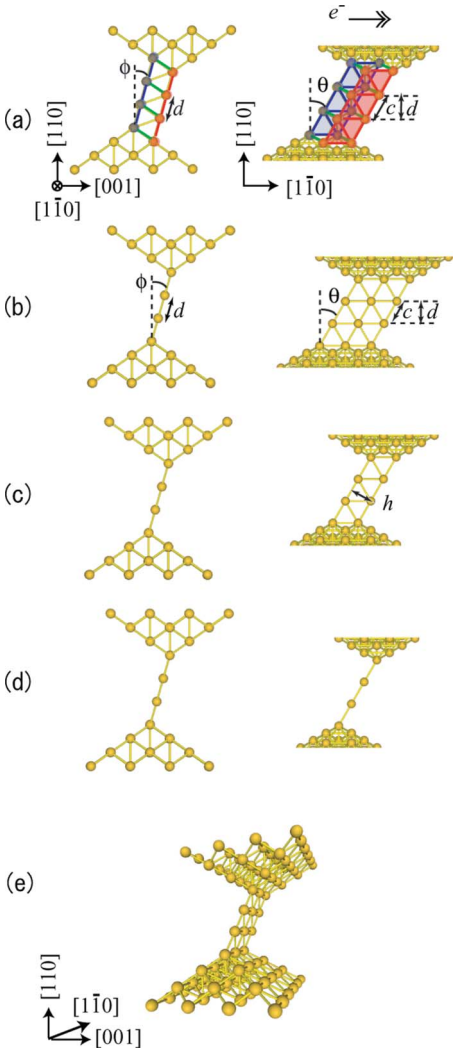

FIG. 6. (Color online) (a) Quadruple, (b) triple, (c) double, (d) single chain models; top view in the left column, and side view in the right column. Note that the number of atomic chains is seen in the side view. Note also that (a)–(d) are responsible to TEM images shown in Figs. 5(a)–5(d), respectively. (e) Birds-eye view of the triple atomic chain model. c is intrachain spacing and h is interchain spacing.

6(a)–6(d). Quadruple, triple, double, and single chain models are presented in Fig. 6. The three-dimensional configuration of the chain models are illustrated using the top view and the side view. The ⟨110⟩ atomic rows are arranged in a zigzag configuration that resembles the (111) atomic sheet of crystalline gold. When $\theta=30°$ and $\phi=15.75°$, the nanowire and the electrode have a twin relation [see birds-eye view in Fig. 6(e)]. Assuming this inclined angle θ and the intrachain spacing of $c=0.288$ nm, the distance between the dark dots $d(=c/\cos\theta)$ is estimated to be 0.25 nm (see side view in Fig. 6). This model corresponds well with the observed ranges of d and ϕ. Simulated TEM images for the model structures, shown in the inset in Fig. 5, agree well quantitatively with observations.

C. Conductance of (n,m,l) nanowire with hexagonal cross section

Figure 7(a) schematically illustrates the hexagonal cross-sectional structure of a gold [110] nanowire.[33] The structure is designated as an (n,m,l) cross section, where n is the number of $(\bar{1}11)$ planes and m is the number of $(1\bar{1}1)$ planes, and l is the number of (001) planes, as shown in the figure. When the nanowire with an (n,m,l) cross section is imaged by an electron beam irradiated along the $[\bar{1}0\bar{1}]$ direction, the number of $(\bar{1}11)$ planes, n, is seen directly in the TEM image, such as shown in Fig. 7(b). However, m and n values are not known from the TEM images. Therefore, while TEM images show a constant number of n planes, the time-evolution conductance can display multiple values, depending on m and/or l values. Similarly, when the (n,m,l) nanowire is imaged from the $[\bar{1}10]$ direction, the number of the (001) plane, l, is known, as shown in Fig. 7(c). Time-evolution conductance for a constant number of l planes can yield multiple values, depending on the invisible change of n and/or m values.

We constructed a partial conductance histogram, $G(n)$, in a following manner. In each of the 250 conductance curves among the total 300 ones, the part in which the corresponding TEM image showed n planes was selected. Each partial conductance histogram, $G(n)$, for $n=3-9$ was obtained by

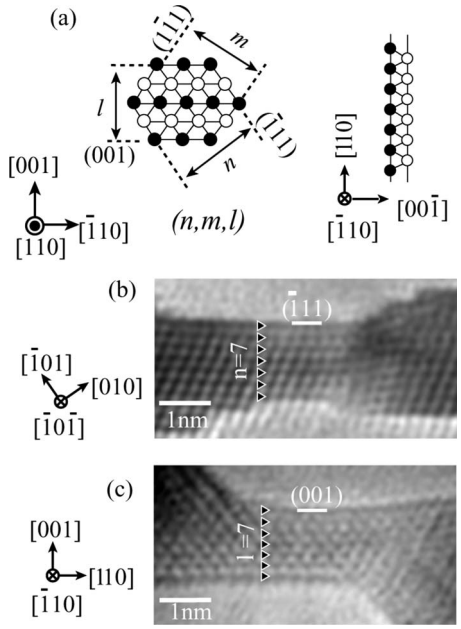

FIG. 7. (a) Cross-section (left) and side view (right) of the schematic representation of gold [110] nanowire. The cross section has hexagonal (n,m,l) structure; n represents the number of $(\bar{1}11)$ planes and m, the number of $(1\bar{1}1)$ ones, while l represents the number of (001) ones. A pair of open and solid circles represents different stacking planes along the [110] wire axis. (b) TEM image of the gold [110] nanowire viewed from the $[\bar{1}0\bar{1}]$ direction, and (c) TEM image viewed from the $[\bar{1}10]$ direction.

building up these parts as shown in Fig. 8(a). Similarly, from the 50 among the total curves, each partial conductance histogram, $G(l)$, for $l=3-9$ was obtained as shown in Fig. 8(b). Each partial conductance histogram shows several peaks. For example, the peaks in $G(n=7)$ correspond to $(7,m,l)$ cross sections with unknown m and l values. Taking into account the fact that the nanowire of a (n,m,l) cross section has a unique conductance value, we looked for the coincident peak with the same conductance value in $G(n)$ and $G(l)$. Among

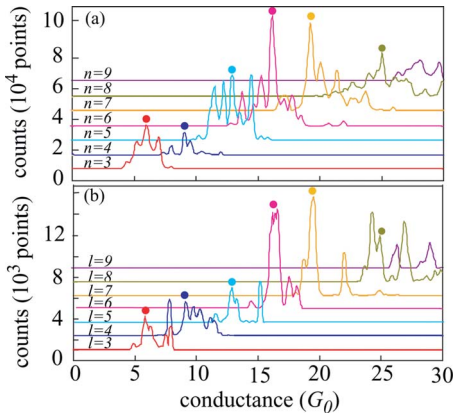

FIG. 8. (Color online) (a) Partial conductance histogram, $G(n)$. (b) Partial conductance histogram, $G(l)$. Note that the peak marked by the solid circle in $G(n=7)$ (orange curve) is recognizable in $G(l=7)$ at the same conductance value, but never in the other $G(n)$ and $G(l)$ curves.

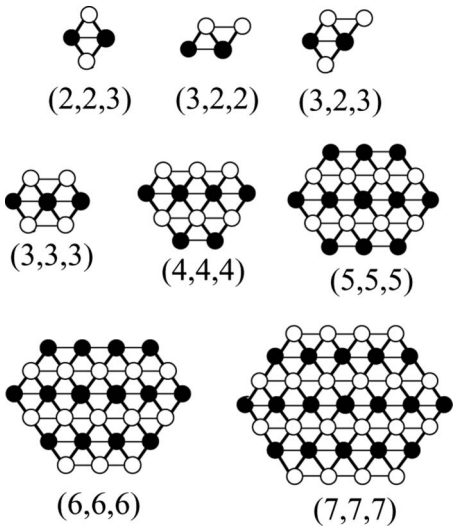

FIG. 9. Models in cross sections of hexagonal (n,m,l) structures. Open and solid circles represent [110] atomic rows, which are arranged similar to the (110) lattice planes of bulk gold crystal. The (2,2,3) and (3,2,2) are rhombic and parallelepiped structures, respectively. For $n>3$, only (n,n,n) are illustrated.

the coincident peaks in the histograms of Fig. 8, those of $n=l$ are high and noticeable as marked by solid circles. These correspond to the (n,m,n) cross sections, wherein m remains unsettled. The (n,m,n) peaks do not correspond with any of the peaks in the partial histogram of $G(n-1)$ and $G(n+1)$. The $(7,m,7)$ peak, for example, has no coincident peak either in $G(n=6)$ or in $G(n=8)$. Taking the geometrical degeneracy between n and m into account, the coincident $(7,m,7)$ peak was determined to have the (7, 7, 7) cross section. Thus, we could assign the peaks for the (3,3,3)–(8,8,8) structures, marked by solid circles in Fig. 3(a). The remaining peaks in Fig. 5(a) correspond to the (n,m,l) cross sections, such as (6,5,6), (6,6,5), and (5,6,5) cross sections.

Figure 9 illustrates the structure of the (n,n,n) cross section. The hexagonal prism structure with the highest symmetry was adopted. The number of atomic rows, N, making up the hexagonal prism cross section then is $N=(3n^2+1)/4$ for odd number n and $N=3n^2/4$ for even number n. Thus N is 7, 12, 19, 27, 37, and 48 for $n=3$, 4, 5, 6, 7, and 8, respectively. Thus the relationship between g and N was derived as summarized in the second and the fourth column of Table I. The observed conductance values are not proportional to N, or the cross-sectional area of the nanowires.

D. Ballistic transport inside nanowires

Figure 10 shows the time evolution of the conductance curve and corresponding TEM images. The TEM images in Figs. 10(b)–10(d) show a process where a $(\bar{1}11)$ plane is removed, and the number of n planes is consequently reduced from 6 to 5. The nanowire in Fig. 10(b) maintains a constant conductance of around $g=13.9$, which sharply decreases to $g=13.0$ as soon as the removal is started at the left electrode. Once the conductance has decreased, it is kept almost constant until the removal is finished in Fig. 10(d).

TABLE I. The relation between peak index (N_p), normalized conductance (g), number of conductance channels (N_c), and number of ⟨110⟩ atomic rows composing nanowire (N).

N_p	1	2	3	4	5	6	7	8	9	10	11	12	13	14	15	16	17	18	19	20	21	22	23	24	25	26	27	28
g	1	1.9	2.7	3.9	5.2	6	7	8	9.1	9.6	10.3	11.6	12.3	13	13.8	14.6	15.3	16.2	17.2	17.7	18.8	19.3	20.1	21.5	22	22.6	23.8	25
N_c	1	2	3	4		6			9					14				18				22						
N	1	2	3	4		7			12					19				27				37						48

Therefore, the gold ⟨110⟩ nanowire itself behaves as a ballistic conductor. The conductance is determined by the number of conductance channels which depend on the narrowest cross-sectional area. A small dip in the conductance plateau, for example, marked label D in Fig. 10(a), was sometimes observed in the time-evolution conductance curves. Such dips had a depth of about $0.3G_0$, and resulted from relative sliding motion at the interface between the nanowire and electrode.

In the thinning processes, stacking faults occasionally appeared and/or disappeared in the nanowires. Figure 11(a) shows a stacking fault that crosses over a ⟨110⟩ nanowire. Figure 11(b) shows a TEM image after elimination of the stacking fault from the nanowire. The time-dependent conductance curve corresponding to this change is shown in Fig. 11(c). The stacking fault is eliminated at the moment indicated by the arrow C. The conductance shows no change before and after the moment of elimination. In other cases, no change in the conductance larger than the experimental error has been detected so far. We therefore conclude that stacking faults have little effect on ballistic conductance of the nanowires.

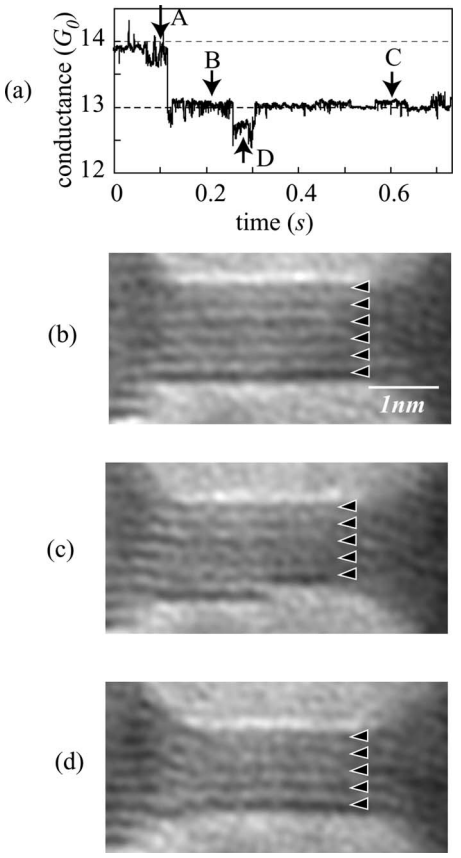

FIG. 10. (a) Time evolution of conductance during thinning of a ⟨110⟩ nanowire. [(b)–(d)] TEM images, taken at times labeled A, B, C in (a), respectively. Note that the sudden jump from $g=13.9$ to 13.0 corresponds to the TEM image change from (b) to (c). Triangle arrow heads indicate the $(\bar{1}11)$ lattice planes. Note also the conductance dip ($g=13.0$ and 12.7) at D.

III. THEORETICAL CALCULATIONS

A. Number of conductance channels

The electronic structure for each structure proposed in this study were calculated using first-principles calculations based on density-functional theory[44,45] within the generalized-gradient approximation (GGA).[46] The electronic structure was calculated for infinite chains or nanowires. The number of conductance channels was evaluated from the

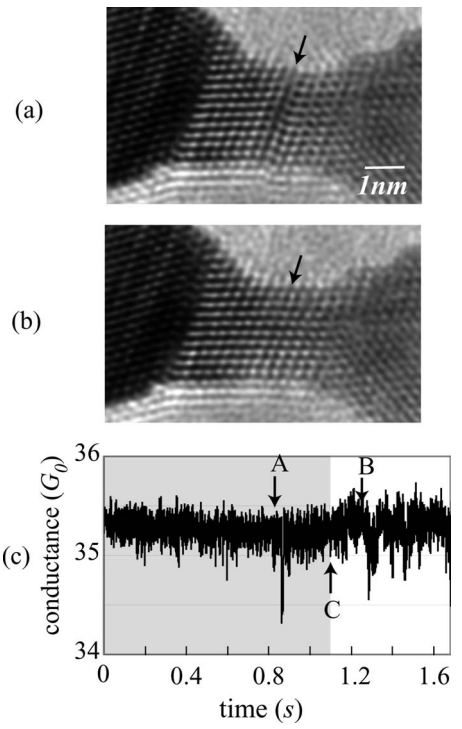

FIG. 11. (a) TEM image of a nanowire with a stacking fault, and (b) after release of the stacking fault. (c) Corresponding time evolution of the conductance. A and B represent time of the recording TEM images (a) and (b), respectively. Note the little change in conductance before and after the release of the stacking fault (shaded and unshaded regions).

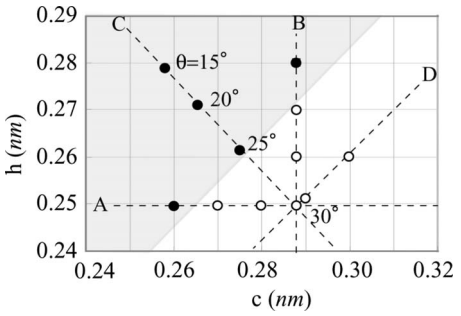

FIG. 12. The number of conductance channels (N_c) of the triple chain structure [Fig. 6(b)] depending on the intrachain spacing, c, and interchain spacing, h. Open circles represent structures having $N_c=2$, while solid circles, those having $N_c=3$. The sheet structure with $c_0=0.288$ nm, $h_0=0.250$ nm, and $\theta=30°$ has the bulk (111) sheet. The structures on line A have a constant interchain spacing, $h=h_0$ ($c=2h_0 \tan\theta$), and those of the line B have a constant intrachain spacing, $c=c_0$ [$h=c_0/(2\tan\theta)$]. The structures on line C have $c=h_0/\cos\theta$ and $h=c_0\cos\theta$, and those of line D have $\theta=30°$. Note that the sheet structures on A(b), C, and D have centered rectangular, oblique, and hexagonal symmetry, respectively.

number of electronic bands crossing the Fermi level. A single atomic chain gave one conductance channel, assuming that the intra-atomic spacing is equal to the nearest-neighbor atomic distance for bulk gold crystal of $c=0.288$ nm. Double chains, with a zigzag configuration of the (111) sheets in crystalline gold, had two conductance channels. However, triple chains had two or three conductance channels depending on the interchain spacing, h, or the intrachain spacing, c, as shown in Fig. 12. They had three channels when the intrachain spacing, c, was shortened by more than 0.03 nm, or the interchain spacing, h, expanded by more than 0.03 nm relative to the bulk (111) sheet. For quadruple chains, the parallelepiped configuration yielded four channels (see Fig. 9). On the other hand, the rhombic cross section gave three channels. The hexagonal (n,n,n) structure, which has the same unit cell as the bulk gold structure, had 6, 9, 14, 18, and 22 channels for $n=3$, 4, 5, 6, and 7, respectively. Figures 13(a)–13(f) show the isosurface images of the electron density for the six open conductance channels in the (3, 3, 3) structure. Density of electron of each conductance channel was delocalized over seven atomic rows. Therefore, each conductance channel was not associated with individual atomic chains.

B. Comparison with experimental results

Table I summarizes the peak index in the conductance histogram (N_p), the normalized conductance value ($g=G/G_0$), the number of the conductance channel (N_c), and the number of the ⟨110⟩ atomic rows composing nanowire (N). The number of the conductance channel is found to agree well with the peak index. This suggests that each peak appears whenever each conductance channel opens one by one. Then, the ⟨110⟩ nanowires transport carriers ballistically. As shown in Fig. 3, the observed conductance value, g, is almost the same as the number of the conductance channel in $g<10$, however, it is lower than the number of the conductance channel in $g>10$. Following the Landauer formula, $g=\Sigma_j T_j$, where T_j is the transmission probability of the jth conductance channel. The transmission probability per channel, $\langle T\rangle=\Sigma_j T_j/\Sigma_j$, is obtained by dividing the conductance value by the peak index as shown in Fig. 14. The figure shows that transmission is almost perfect for thin nanowires for $g<10$, while it gradually decreases for $g>10$. For thicker nanowires, the $\langle T\rangle$ becomes about 0.9.

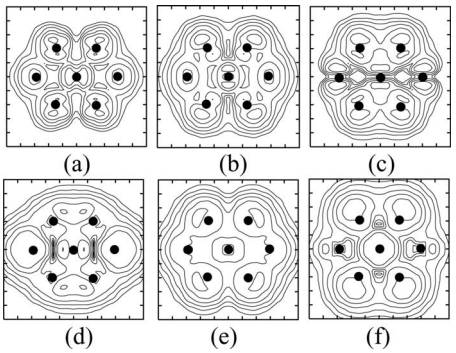

FIG. 13. [(a)–(f)] Isosurface images of the electron densities for six open conductance channels in hexagonal (3,3,3) structure, respectively. The dots represent positions of the [110] atomic rows. Contour lines correspond to 0.25, 0.5, 1.0, 2.0, 4.0, and 8.0($\times 10^{-3}$ bohr^{-3}) from the outside. The density of electrons is averaged along the wire axis. Six conductance channels are open, and (a) is the lowest energy state.

Figure 15 shows the relationship between the number of conductance channels and the cross-sectional area of the gold ⟨110⟩ nanowire. The cross-sectional area is obtained by multiplying the number of atomic rows, N, by the area per atomic row, $s_0=a^2/(2\sqrt{2})$, where $a=0.408$ nm is the lattice constant of the bulk gold crystal at room temperature. For comparison, the number of conductance channels is estimated using corrected Sharvin equation based on a semiclassical approximation,[47] $N_c=\pi S/\lambda_F^2-\sqrt{\pi S}/\lambda_F+1/6$, where S is the cross section of the nanowire and λ_F is the Fermi wavelength. For thinner nanowire ($N_c\leq 20$), the number of conductance channels obtained experimentally is larger than one obtained from the corrected Sharvin formula. This discrepancy may come from smearing-out effect of electrons.[48] For thick nanowire ($N_c\geq 20$), experimental and semiclassical numbers of conductance channels accord with each other.

IV. DISCUSSION

A. Preferred peaks and the number of conductance channels

The present experiment was carried out by selecting gold ⟨110⟩ nanowires. It was first shown that no missing integer

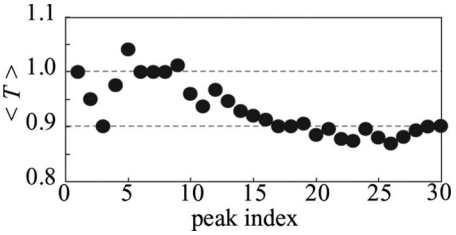

FIG. 14. Transmission probability per channel, $\langle T\rangle$, in relation to the peak index. $\langle T\rangle=g/N_p$ is calculated using Table I.

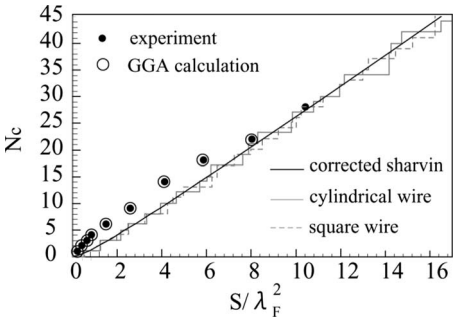

FIG. 15. Relationship between the cross-sectional area and the number of conductance channels of the gold ⟨110⟩ nanowire. Solid and open circles are plots of the experimental and calculated number of the conductance channels, N_c, in Table I. $S=a^2N/(2\sqrt{2})$ and $\lambda_F=0.52$ nm are cross-sectional area and Fermi wavelength, respectively, where N is number of atomic rows and $a=0.408$ nm is the lattice constant of the bulk gold crystal. The solid line is the corrected Sharvin formula, $N_c=\pi S/\lambda_F^2+\sqrt{\pi S}/\lambda_F+1/6$. For reference, the number of conductance channels for cylindrical or for the square cross section was calculated. Gray and dotted lines represent the semiclassical calculation for cylindrical and square cross sections, respectively.

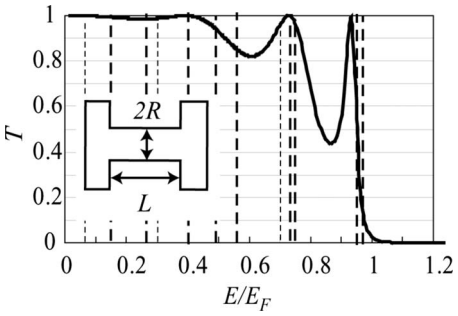

FIG. 16. Transmission probability $T(E,L)$ as a function of E, for a cylindrical nanowires of length $L=1$ nm, radius $R=0.83$ nm, and the Fermi energy $E_F=5.53$ eV. Dotted and dashed lines indicate the energy of transversely confined states, E. Dashed lines show degenerate states and dotted lines, nondegenerate states. Note that the decrease in transmission probability for E slightly below the Fermi level.

number existed in the quantum state for the conductance channel, and the conductance channel increased one by one. Second, the nanowire was seen to behave as a ballistic conductor. Third, partial transmission cannot be disregarded for thicker nanowires, and the apparent conductance is smaller than the number of conductance channels in this case.

The present observations are different from previous ones.[28–30] Mares and co-workers[28,29] proposed, based on their conductance histograms, that thin gold nanowires preferred the electronic shell structure, whereas thicker nanowires preferred the atomic-shell structure. The atomic-shell model insisted that the hexagonal (3,3,3), (5,5,5), and (7,7,7) structures gave main peaks in their conductance histogram, and a subsidiary peak arose whenever a monoatomic layer was attached (detached) on one of the six side faces. Their conductance values, therefore, were determined by the geometry or cross-sectional area. The conductance values responsible for their peaks, which do not increase in steps of the conductance quantum, disagree with our present observations.

The square root of their conductance value changed linearly with an increase in their peak index, whose slope showed a break at around $g=10$ (e.g., Fig. 4 in Ref. 29). This break has been interpreted as being due to evolution of the atomic-shell structure. In the present study, the plot of conductance vs peak index [Fig. 3(b)] shows a break around $g=10$, but this is presumably caused by partial transmission of the conductance channel. Furthermore, no critical change in the cross-sectional structure is recognizable at around $g=10$. In fact, the present gold ⟨110⟩ nanowires giving the preferred peaks have quantum states equal to the number of conductance channels, that is, the peak index.

B. Partial transmission probability

According to the present results, the transmission probability decreases for thick nanowires. For a model incorporating a narrow cylindrical rod (nanowire) connected with two wider cylindrical rods (electrodes), it was demonstrated that the partial transmission depended on the length and cross-sectional area of the rod (nanowire).[49,50] Provided that an eigenstate of electrons confined transversely in a nanowire has energy E, the number of the discrete states below the Fermi energy E_F corresponds to the number of conductance channels. Based on the simple jellium model,[51] the transmission probability of a conductance channel, T, as a function of E, and length of nanowire, L, is given by

$$T(E,L)=\left[1+\frac{E^2}{4E_F(E_F-E)}\sin^2(kL)\right]^{-1}, \qquad (1)$$

where $k^2=(2m/\hbar^2)(E_F-E)$. Figure 16 shows $T(E,L)$ in relation to E for a cylindrical rod. For a conductance channel with a confined state slightly below the Fermi energy, the transmission probability, T, is reduced due to multiple reflection of electrons at nonadiabatic interface between the nanowire and electrodes. In this model, the conductance value given by the 21 conductance channels is calculated to be $g=18.1$. The conductance reduction from the quantized conductance value is attributed to reducing the transmission probabilities of the conductance channels corresponding to the confined states slightly below the Fermi energy. As the cross section increases, the number of the confined states just below the Fermi energy increases. They suffer sever drop of their transmission probability. For each size of cylindrical rods, calculated conductance values were plotted in Fig. 3(a) in relation to the number of conductance channels (peak indices). Although, in this model, the transmission probability is almost one when $kL=n\pi$, this 100% transmission is not occurred perfectly but partially (partial coherence). Because the conductance of the ⟨110⟩ nanowires in Figs. 10(c) and 10(d) show no noticeable change for the length difference of about 1 nm (about four atomic distances, 0.288 nm×4). Even when a nanowire was thinned partly by one or two atomic distances, the conductance change (or fluctuation) did not exceed about $0.4G_0$. For the present ⟨110⟩ nanowires of different lengths with the same cross section, the conductance values are varied not more than $0.4G_0$, as seen in the

partial conductance histogram. The partial coherency of the ⟨110⟩ nanowire is in agreement with the report suggesting that the phase coherence length is about 1 nm at room temperature.[52]

C. Stable nanowire

The sheet structures and (n,n,n) hexagonal prism structures observed in the present study gave conspicuous preferred peaks in the conductance histogram. These structures did not only have frequent appearance in the *in situ* TEM experiments, but they also had long-lasting plateaus in the time-evolution experiments. Therefore, the atomic configurations summarized in Figs. 6 and 9 must be stable structures. In theoretical arguments regarding the stability of nanowires and/or stable structures, free energy[53,54] or tension[54,55] have been discussed. As proposed,[27] a stable nanowire accommodates its structure to maximize the number of conductance channels. Because the conductance channel serves as the metallic bonds connecting the nanowire to the electrodes.[56] In the present study, the quadruple chains were found to have the parallelepiped configuration [see Fig. 6(a) and 9] corresponding to the peak at $g=4$. The quadruple chains with rhombic configuration (see Fig. 9), which was calculated to have $g=3$,[36] was not observed in our *in situ* TEM observations. Another example is the case of the triple chain structure with sheet configuration. Triple chain structures that have atomic arrangements of the hexagonal symmetry were calculated to have $g=2$. Triple chains take $g=3$ after deformation of the intrachain and interchain spacing more than 10% from the bulk spacing, forming structures of the centered rectangular or oblique symmetry. This may accord with the prediction that gold nanowires prefer rather elliptical cross section than cylindrical one due to Jahn-Teller effect for $g=3$.[57] Our experiments show that triple and quadruple chains preferred atomic structures of a higher g value. Thus the increment of the number of open channels was thought to be preferred for stability at the cost of strain energy due to structural relaxation.

V. CONCLUSIONS

The conductance quantization of gold ⟨110⟩ nanowires was investigated in the present study. TEM fitted with STM was used to measure the conductance of gold ⟨110⟩ nanowires that were successively formed during the thinning of a gold contact. A series of peaks appeared in the conductance histogram from 300 thinning processes. The conductance value for each peak corresponded to the respective structures of the nanowire. Among 30 peaks in a conductance range below $28G_0$, four peaks at $1.0G_0$, $1.9G_0$, $2.7G_0$, and $3.9G_0$ were found to be related to the atomic chain and atomic sheets, and the other 26 peaks above $4G_0$ were related to the (n,m,l) hexagonal prism structures. Based on the determined structures, the number of conductance channels was calculated by first-principles theory, which coincided with the indices of the 30 peaks. In conclusion, we found that the conductance quantum was introduced one by one into the nanowires, whenever the nanowire changed its structure. The preferred nanowires behaved like ballistic conductor. The transmission probability per conductance channel, however, became 0.9 for $g>10$. This reduction was explained by lowering the transmission probabilities of the conductance channels having the confined states slightly below the Fermi energy.

ACKNOWLEDGMENTS

We thank Y. Tanishiro for a helpful discussion. This work was supported by the Global COE program at TokyoTech "Nanoscience and Quantum Physics" by the Ministry of Education, Culture, Sports, Science and Technology of Japan.

*oshima.y.aa@m.titech.ac.jp
†http://wwwsurf.phys.titech.ac.jp/tylab/index_e.html.

[1] N. Agraït, A. Levy Yeyati, and J. M. van Ruitenbeek, Phys. Rep. **377**, 81 (2003).
[2] J. I. Pascual, J. Mendéz, J. Gómez-Herrero, A. M. Baró, N. García, Vu Thien Binh, Phys. Rev. Lett. **71**, 1852 (1993).
[3] N. Agraït, J. G. Rodrigo, and S. Vieira, Phys. Rev. B **47**, 12345 (1993).
[4] J. M. Krans, J. M. van Ruitenbeek, V. V. Flsun, I. K. Yanson, and L. J. de Jongh, Nature (London) **375**, 767 (1995).
[5] A. I. Yanson, I. K. Yanson, and J. M. van Ruitenbeek, Nature (London) **400**, 144 (1999).
[6] M. Brandbyge, J. Schiøtz, M. R. Sørensen, P. Stoltze, K. W. Jacobsen, J. K. Nørskov, L. Olesen, E. Lægsgaard, I. Stensgaard, and F. Besenbacher, Phys. Rev. B **52**, 8499 (1995).
[7] C. J. Muller, J. M. Krans, T. N. Todorov, and M. A. Reed, Phys. Rev. B **53**, 1022 (1996).
[8] J. L. Costa-Krämer, N. García, and H. Olin, Phys. Rev. B **55**, 12910 (1997).
[9] K. Hansen, E. Lægsgaard, I. Stensgaard, and F. Besenbacher, Phys. Rev. B **56**, 2208 (1997).
[10] B. Ludoph, M. H. Devoret, D. Esteve, C. Urbina, and J. M. van Ruitenbeek, Phys. Rev. Lett. **82**, 1530 (1999).
[11] B. Ludoph and J. M. van Ruitenbeek, Phys. Rev. B **61**, 2273 (2000).
[12] L. Olesen, E. Lægsgaard, I. Stensgaard, F. Besenbacher, J. Schiøtz, P. Stoltze, K. W. Jacobsen, and J. K. Nørskov, Phys. Rev. Lett. **74**, 2147 (1995).
[13] E. Scheer, P. Joyez, D. Esteve, C. Urbina, and M. H. Devoret, Phys. Rev. Lett. **78**, 3535 (1997).
[14] A. I. Yanson and J. M. van Ruitenbeek, Phys. Rev. Lett. **79**, 2157 (1997).
[15] S. K. Nielsen, Y. Noat, M. Brandbyge, R. H. M. Smit, K. Hansen, L. Y. Chen, A. I. Yanson, F. Besenbacher, and J. M. van Ruitenbeek, Phys. Rev. B **67**, 245411 (2003).
[16] B. Ludoph, N. van der Post, E. N. Bratus', E. V. Bezuglyi, V. S. Shumeiko, G. Wendin, and J. M. van Ruitenbeek, Phys. Rev. B **61**, 8561 (2000).

[17] U. Landman, W. D. Luedtke, N. A. Burnham, and R. J. Colton, Science **248**, 454 (1990).
[18] T. N. Todorov and A. P. Sutton, Phys. Rev. Lett. **70**, 2138 (1993).
[19] A. M. Bratkovsky, A. P. Sutton, and T. N. Todorov, Phys. Rev. B **52**, 5036 (1995).
[20] U. Landman, W. D. Luedtke, B. E. Salisbury, and R. L. Whetten, Phys. Rev. Lett. **77**, 1362 (1996).
[21] M. R. Sørensen, M. Brandbyge, and K. W. Jacobsen, Phys. Rev. B **57**, 3283 (1998).
[22] H. Mehrez and S. Ciraci, Phys. Rev. B **56**, 12632 (1997).
[23] M. Dreher, F. Pauly, J. Heurich, J. C. Cuevas, E. Scheer, and P. Nielaba, Phys. Rev. B **72**, 075435 (2005).
[24] H. Ohnishi, Y. Kondo, and K. Takayanagi, Nature (London) **395**, 780 (1998).
[25] M. Okamoto and K. Takayanagi, Phys. Rev. B **60**, 7808 (1999).
[26] H. Hakkinen, R. N. Barnett, A. G. Scherbakov, and U. Landman, J. Phys. Chem. B **104**, 9063 (2000).
[27] Y. Kurui, Y. Oshima, M. Okamoto and K. Takayanagi, Phys. Rev. B **77**, 161403(R) (2008).
[28] A. I. Mares, A. F. Otte, L. G. Soukiassian, R. H. M. Smit, and J. M. van Ruitenbeek, Phys. Rev. B **70**, 073401 (2004).
[29] A. I. Mares and J. M. van Ruitenbeek, Phys. Rev. B **72**, 205402 (2005).
[30] E. Medina, M. Díaz, N. León, C. Guerrero, A. Hasmy, P. A. Serena, and J. L. Costa-Krämer, Phys. Rev. Lett. **91**, 026802 (2003).
[31] G. Rubio, N. Agraït, and S. Vieira Phys. Rev. Lett. **76**, 2302 (1996).
[32] A. I. Yanson, I. K. Yanson, and J. M. van Ruitenbeek, Phys. Rev. Lett. **87**, 216805 (2001).
[33] Y. Kondo and K. Takayanagi, Phys. Rev. Lett. **79**, 3455 (1997).
[34] V. Rodrigues, T. Fuhrer, and D. Ugarte, Phys. Rev. Lett. **85**, 4124 (2000).
[35] Y. Kurui, Y. Oshima, and K. Takayanagi, J. Phys. Soc. Jpn. **76**, 123601 (2007).
[36] L. G. C. Rego, A. R. Rocha, V. Rodrigues, and D. Ugarte, Phys. Rev. B **67**, 045412 (2003).
[37] Y. Oshima, K. Mouri, H. Hirayama, and K. Takayanagi, Surf. Sci. **531**, 209 (2003).
[38] R. Hoffmann, D. Weissenberger, J. Hawecker, and D. Stöffler, Appl. Phys. Lett. **93**, 043118 (2008).
[39] Y. Kondo and K. Takayanagi, Science **289**, 606 (2000).
[40] Y. Oshima, K. Mouri, H. Hirayama, and K. Takayanagi, J. Phys. Soc. Jpn. **75**, 053705 (2006).
[41] Y. Oshima, A. Onga, and K. Takayanagi, Phys. Rev. Lett. **91**, 205503 (2003).
[42] A. I. Yanson, G. Rubio Bollinger, H. E. van den Brom, N. Agraït, and J. M. van Ruitenbeek, Nature (London) **395**, 783 (1998).
[43] H. Koizumi, Y. Oshima, Y. Kondo, and K. Takayanagi, Ultramicroscopy **88**, 17 (2001).
[44] P. Hohenberg and W. Kohn, Phys. Rev. **136**, B864 (1964).
[45] W. Kohn and L. J. Sham, Phys. Rev. **140**, A1133 (1965).
[46] J. P. Perdew, K. Burke, and M. Ernzerhof, Phys. Rev. Lett. **77**, 3865 (1996).
[47] C. Höppler and W. Zwerger, Phys. Rev. Lett. **80**, 1792 (1998).
[48] A. García-Martín, J. A. Torres, and J. J. Sáenz, Phys. Rev. B **54**, 13448 (1996).
[49] J. A. Torres and J. J. Sáenz, J. Phys. Soc. Jpn. **73**, 2182 (2004).
[50] F. Kassubek, C. A. Stafford, and H. Grabert, Phys. Rev. B **59**, 7560 (1999).
[51] L. I. Shiff, Quantum Mechanics.
[52] S. Friedrichowski and G. Dumpich, Phys. Rev. B **58**, 9689 (1998).
[53] O. Gülseren, F. Ercolessi, and E. Tosatti, Phys. Rev. Lett. **80**, 3775 (1998).
[54] D. Cheng, W. Y. Kim, S. K. Min, T. Nautiyal, and K. S. Kim, Phys. Rev. Lett. **96**, 096104 (2006).
[55] E. Tosatti, S. Prestipino, S. Kostlmeier, A. Dal Corso, and F. D. Di Tolla, Science **291**, 288 (2001).
[56] C. A. Stafford, D. Baeriswyl, and J. Bürki, Phys. Rev. Lett. **79**, 2863 (1997).
[57] D. F. Urban, J. Bürki, C.-H. Zhang, C. A. Stafford, and H. Grabert, Phys. Rev. Lett. **93**, 186403 (2004).